

# The VIMOS Ultra-Deep Survey (VUDS): fast increase in the fraction of strong Lyman- $\alpha$ emitters from $z = 2$ to $z = 6$ <sup>\*</sup>

P. Cassata<sup>1,2</sup>, L. A. M. Tasca<sup>1</sup>, O. Le Fèvre<sup>1</sup>, B. C. Lemaux<sup>1</sup>, B. Garilli<sup>3</sup>, V. Le Brun<sup>1</sup>, D. Maccagni<sup>3</sup>, L. Pentericci<sup>5</sup>, R. Thomas<sup>1</sup>, E. Vanzella<sup>4</sup>, G. Zamorani<sup>4</sup>, E. Zucca<sup>4</sup>, R. Amorin<sup>5</sup>, S. Bardelli<sup>4</sup>, P. Capak<sup>13</sup>, L. P. Cassara<sup>3</sup>, M. Castellano<sup>5</sup>, A. Cimatti<sup>6</sup>, J. G. Cuby<sup>1</sup>, O. Cucciati<sup>6,4</sup>, S. de la Torre<sup>1</sup>, A. Durkalec<sup>1</sup>, A. Fontana<sup>5</sup>, M. Giavalisco<sup>14</sup>, A. Grazian<sup>5</sup>, N. P. Hathi<sup>1</sup>, O. Ilbert<sup>1</sup>, C. Moreau<sup>1</sup>, S. Paltani<sup>10</sup>, B. Ribeiro<sup>1</sup>, M. Salvato<sup>15</sup>, D. Schaerer<sup>11,9</sup>, M. Scodeggio<sup>3</sup>, V. Sommariva<sup>6,5</sup>, M. Talia<sup>6</sup>, Y. Taniguchi<sup>16</sup>, L. Tresse<sup>1</sup>, D. Vergani<sup>7,4</sup>, P. W. Wang<sup>1</sup>, S. Charlot<sup>8</sup>, T. Contini<sup>9</sup>, S. Fotopoulou<sup>10</sup>, A. M. Koekemoer<sup>17</sup>, C. López-Sanjuan<sup>11,12</sup>, Y. Mellier<sup>8</sup>, and N. Scoville<sup>13</sup>

<sup>1</sup> Aix Marseille Université, CNRS, LAM (Laboratoire d'Astrophysique de Marseille) UMR 7326, 13388 Marseille, France  
e-mail: paolo.cassata@lam.fr

<sup>2</sup> Instituto de Física y Astronomía, Facultad de Ciencias, Universidad de Valparaíso, Gran Bretaña 1111, Playa Ancha, Valparaso, Chile

<sup>3</sup> INAF-IASF, via Bassini 15, 20133 Milano, Italy

<sup>4</sup> INAF-Osservatorio Astronomico di Bologna, via Ranzani, 1, 40127 Bologna, Italy

<sup>5</sup> INAF-Osservatorio Astronomico di Roma, via di Frascati 33, 00040 Monte Porzio Catone, Italy

<sup>6</sup> University of Bologna, Department of Physics and Astronomy (DIFA), V.le Berti Pichat, 6/2, 40127 Bologna, Italy

<sup>7</sup> INAF-IASF Bologna, via Gobetti 101, 40129 Bologna, Italy

<sup>8</sup> Institut d'Astrophysique de Paris, UMR 7095 CNRS, Université Pierre et Marie Curie, 98 bis Boulevard Arago, 75014 Paris, France

<sup>9</sup> Institut de Recherche en Astrophysique et Planétologie, IRAP, CNRS, Université de Toulouse, UPS-OMP, 14 avenue E. Belin, 31400 Toulouse, France

<sup>10</sup> Department of Astronomy, University of Geneva ch. d'Écogia 16, 1290 Versoix, Switzerland

<sup>11</sup> Geneva Observatory, University of Geneva, ch. des Maillettes 51, 1290 Versoix, Switzerland

<sup>12</sup> Centro de Estudios de Física del Cosmos de Aragón, Teruel, Spain

<sup>13</sup> Department of Astronomy, California Institute of Technology, 1200 E. California Blvd., MC 249-17, Pasadena, CA 91125, USA

<sup>14</sup> Astronomy Department, University of Massachusetts, Amherst, MA 01003, USA

<sup>15</sup> Max-Planck-Institut für Extraterrestrische Physik, Postfach 1312, 85741 Garching bei München, Germany

<sup>16</sup> Research Center for Space and Cosmic Evolution, Ehime University, Bunkyo-cho 2-5, 790-8577 Matsuyama, Japan

<sup>17</sup> Space Telescope Science Institute, 3700 San Martin Drive, Baltimore, MD 21218, USA

Received 17 March 2014 / Accepted 15 September 2014

## ABSTRACT

**Aims.** The aim of this work is to constrain the evolution of the fraction of strong Ly $\alpha$  emitters among UV selected star-forming galaxies at  $2 < z < 6$ , and to measure the stellar escape fraction of Ly $\alpha$  photons over the same redshift range.

**Methods.** We exploit the ultradeep spectroscopic observations with VIMOS on the VLT collected by the VIMOS Ultra-Deep Survey (VUDS) to build an unique, complete, and unbiased sample of  $\sim 4000$  spectroscopically confirmed star-forming galaxies at  $2 < z < 6$ . Our galaxy sample includes UV luminosities brighter than  $M_{\text{FUV}}^*$  at  $2 < z < 6$ , and luminosities down to one magnitude fainter than  $M_{\text{FUV}}^*$  at  $2 < z < 3.5$ .

**Results.** We find that 80% of the star-forming galaxies in our sample have  $EW_0(\text{Ly}\alpha) < 10 \text{ \AA}$ , and correspondingly  $f_{\text{esc}}(\text{Ly}\alpha) < 1\%$ . By comparing these results with the literature, we conclude that the bulk of the Ly $\alpha$  luminosity at  $2 < z < 6$  comes from galaxies that are fainter in the UV than those we sample in this work. The strong Ly $\alpha$  emitters constitute, at each redshift, the tail of the distribution of the galaxies with extreme  $EW_0(\text{Ly}\alpha)$  and  $f_{\text{esc}}(\text{Ly}\alpha)$ . This tail of large  $EW_0(\text{Ly}\alpha)$  and  $f_{\text{esc}}(\text{Ly}\alpha)$  becomes more important as the redshift increases, and causes the fraction of strong Ly $\alpha$  with  $EW_0(\text{Ly}\alpha) > 25 \text{ \AA}$  to increase from  $\sim 5\%$  at  $z \sim 2$  to  $\sim 30\%$  at  $z \sim 6$ , with the increase being stronger beyond  $z \sim 4$ . We observe no difference, for the narrow range of UV luminosities explored in this work, between the fraction of strong Ly $\alpha$  emitters among galaxies fainter or brighter than  $M_{\text{FUV}}^*$ , although the fraction for the faint galaxies evolves faster, at  $2 < z < 3.5$ , than for the bright ones. We do observe an anticorrelation between  $E(B - V)$  and  $f_{\text{esc}}(\text{Ly}\alpha)$ : generally galaxies with high  $f_{\text{esc}}(\text{Ly}\alpha)$  also have small amounts of dust (and vice versa). However, when the dust content is low ( $E(B - V) < 0.05$ ) we observe a very broad range of  $f_{\text{esc}}(\text{Ly}\alpha)$ , ranging from  $10^{-3}$  to 1. This implies that the dust alone is not the only regulator of the amount of escaping Ly $\alpha$  photons.

**Key words.** galaxies: evolution – galaxies: formation – galaxies: high-redshift – galaxies: fundamental parameters – cosmology: observations

## 1. Introduction

Narrowband surveys targeting the strong Ly $\alpha$  emission from star-forming galaxies (Lyman- $\alpha$  emitters, LAEs; Partridge & Peebles 1967; Djorgovski et al. 1985; Cowie & Hu 1998; Hu et al. 2004; Kashikawa et al. 2006; Gronwall et al. 2007;

<sup>\*</sup> Based on data obtained with the European Southern Observatory Very Large Telescope, Paranal, Chile, under Large Program 185.A-0791.

Murayama et al. 2007; Ouchi et al. 2008; Nilsson et al. 2009) and broadband surveys targeting the deep Lyman break (LBG; Steidel et al. 1999; Bouwens & Illingworth 2006; Bouwens et al. 2010; McLure et al. 2011) have been very successful at exploring the high-redshift Universe. However, the overlap between the populations selected by the two techniques is still debated: LAEs are claimed to be forming stars at rates of  $1\text{--}10 M_{\odot} \text{ yr}^{-1}$  (Cowie & Hu 1998; Gawiser et al. 2006; Pirzkal et al. 2007), to have stellar masses on the order of  $10^8\text{--}10^9 M_{\odot}$  and to have ages smaller than 50 Myr (Pirzkal et al. 2007; Gawiser et al. 2007; Nilsson et al. 2009), while LBGs have in general a broader range of properties (Reddy et al. 2006; Hathi et al. 2012; Schaerer et al. 2011; but see also Kornei et al. 2010).

Steidel et al. (2000) and Shapley et al. (2003) showed that only  $\sim 20\%$  of  $z \sim 3$  LBGs have a Ly $\alpha$  emission strong enough to be detected with the narrowband technique. Recently, many authors have investigated the evolution with the redshift of the fraction of strong Ly $\alpha$  emitters among LBG galaxies. Stark et al. (2010, 2011) showed that this fraction evolves with redshift, and that the overall fraction is smaller (and that the rate of evolution is slower) for UV bright galaxies ( $-21.75 < M_{\text{UV}} < -20.25$ ) than for UV faint ( $-20.25 < M_{\text{UV}} < -18.75$ ) galaxies; they find that the fraction of UV faint galaxies with strong ( $EW_0(\text{Ly}\alpha) > 25 \text{ \AA}$ ) Ly $\alpha$  emission is around 20% at  $z \sim 2\text{--}3$  and reaches  $\sim 50\text{--}60\%$  at  $z \sim 6$ . At higher redshift ( $z > 6\text{--}8$ ), many authors claim a sudden drop in the fraction of spectroscopically confirmed LBGs with strong Ly $\alpha$  emission (Fontana et al. 2010; Pentericci et al. 2011; Ono et al. 2012; Schenker et al. 2012; Caruana et al. 2014), interpreting this as the observational signature of the increasing fraction of neutral hydrogen between  $z \sim 6$  and  $z \sim 7$  due to the tail end of the reionization, although Dijkstra et al. (2014) has argued that the effect can be due to a variation of the average escape fraction over the same redshift range.

However, the bulk of studies of the Ly $\alpha$  fraction at  $3 < z < 8$  (Stark et al. 2010, 2011; Pentericci et al. 2011) are based on a hybrid photometric-spectroscopic technique: the denominator of the fraction (i.e., the *total* number of star-forming galaxies at those redshifts) is only constrained by photometry, and thus its determination relies on the strong assumption that the contamination by low- $z$  interlopers and incompleteness are fully understood and well controlled. The numerator of the fraction is the number of the LBGs that are observed with spectroscopy, and for which a strong Ly $\alpha$  rest-frame Equivalent Width ( $EW_0 > 25 \text{ \AA}$ ) is measured. In fact, the LBGs for which this experiment is done have a UV continuum that is generally too faint to be detected, even with the most powerful spectrographs on 10-meter class telescopes. Recently, Mallery et al. (2012) combined a sample of LAEs and LBGs to constrain the evolution of this fraction, confirming earlier results by Stark et al. (2010, 2011). Given the nature of the selection of these samples, it is important to make a robust estimate of the evolution of the Ly $\alpha$  fraction covering as wide a range in redshift as possible, and based on larger samples.

The Ly $\alpha$  is interesting not only because it allows for the exploration of the high-redshift universe. In fact, its observed properties can give a lot of information about the physical condition of star-forming galaxies. Ly $\alpha$  is thought to be mainly produced by star formation, as the contribution of AGN activity to the Ly $\alpha$  population at  $z < 4$  is found to be less than 5% (Gawiser et al. 2006; Ouchi et al. 2008; Nilsson et al. 2009; Hayes et al. 2010). Because of its resonant nature, Ly $\alpha$  photons are easily scattered, shifted in frequency, and absorbed by the neutral hydrogen and/or by the dust. As a result, in general, Ly $\alpha$  emission

is more attenuated than other UV photons, with the Ly $\alpha$  escape fraction (i.e., the fraction of the Ly $\alpha$  photons that escape the galaxies) that depends strongly on the relative kinematics of the HII and HI regions, dust content, and geometry (Giavalisco et al. 1996; Kunth et al. 1998; Mas-Hesse et al. 2003; Deharveng et al. 2008; Hayes et al. 2014). As a result of their nature, Ly $\alpha$  photons are found to be scattered at much larger scales than UV photons (Steidel et al. 2011; Momose et al. 2014).

Predicting the escape fraction of the Ly $\alpha$  photons as a function of the galaxy properties involves including all the complex effects of radiative transfer of such photons. Developing the first models by Charlot & Fall (1993), Verhamme et al. (2006, 2008, 2012) and Dijkstra et al. (2006, 2012) made huge progress in predicting the shape of the Ly $\alpha$  emission as a function of the properties of the ISM, the presence of inflows/outflows, and dust. Verhamme et al. (2006, 2008) predicted a correlation between  $f_{\text{esc}}(\text{Ly}\alpha)$  and  $E(B - V)$ , with the escape fraction being higher in galaxies with low dust content. Verhamme et al. (2012) and Dijkstra et al. (2012) studied the escape fraction of Ly $\alpha$  photons through a 3D clumpy medium, constraining the dependence on the column density of neutral hydrogen and on the viewing angle.

A lot of effort has been recently put to constrain the correlation between the Ly $\alpha$  properties and the general properties of star-forming galaxies (e.g., dust attenuation, SFR, stellar mass) in the local Universe. Hayes et al. (2014) and Atek et al. (2014) have found that Ly $\alpha$  photons escape more easily from galaxies with low dust content. At high redshift, although on samples that are much smaller than the one we use in this paper, a similar trend has been found by Kornei et al. (2010) and Mallery et al. (2012), respectively at  $z \sim 3$  and at  $4 < z < 6$ . In this paper, we look for this correlation using a sample that is respectively five and ten times larger than the ones used by Mallery and Kornei.

The aim of this paper is to estimate the evolution of the fraction of strong Ly $\alpha$  emitters as a function of the redshift, exploiting data from the new VIMOS Ultra-Deep Survey (VUDS). The goal is twofold: first, to put on firmer grounds the trends that have been found with photometric LBG samples (Stark et al. 2010, 2011) and improve on the knowledge of the evolution of the Ly $\alpha$  fraction; second, to offer the theoreticians a reference sample of galaxies with robust spectroscopic redshifts, with a well measured  $EW_0(\text{Ly}\alpha)$  distribution. In fact, in this paper, we select a sample of galaxies, sliced in volume limited samples according to different recipes, for which we have a spectroscopic redshift in  $\sim 90\%$  of the cases. The continuum is detected for almost all objects in the sample, thus allowing a robust measurement of the redshift based on the UV absorption features even in absence of Ly $\alpha$ .

Our selection is not based on LBG or narrowband techniques, that are prone to incompleteness and contamination, but it is rather based on the magnitude in the  $i'$ -band and on the photometric redshifts measured on the full spectral energy distribution (SED) of galaxies. The most important point to emphasize is that our flux selection is completely independent of the presence of Ly $\alpha$ , at least up to  $z \sim 5$ , because it enters the photometric  $i'$ -band only at  $z > 5$ : since the  $i'$ -band does not contain the Ly $\alpha$  line, objects with strong Ly $\alpha$  emission have not a boosted  $i'$ -band magnitude. Moreover, when the photo- $z$  are computed, some variable Ly $\alpha$  flux (as for other lines like OII, OIII and H $\alpha$ ) is added to the SED: this ensures that even objects with large Ly $\alpha$  flux are reproduced by the template set that is used to compute the photo- $z$ . This also implies that if our selection is incomplete at some redshift, the incompleteness is also independent of the presence (or absence) of Ly $\alpha$ .

For these reasons, this sample is ideal to study the Ly $\alpha$  properties of a well controlled sample of star-forming galaxies. The fraction of strong Ly $\alpha$  emitters among star-forming galaxies is completely constrained by spectroscopy, as is also the case for non-Ly $\alpha$  emitters.

Throughout the paper, we use a standard Cosmology with  $\Omega_M = 0.3$ ,  $\Omega_\Lambda = 0.7$  and  $h = 0.7$ . Magnitudes are in the AB system.

## 2. Data

The data used in this study are drawn from the VIMOS Ultra-Deep Survey (VUDS), an ESO large program with the aim of collecting spectra and redshifts for around 10 000 galaxies to study early phases of galaxy formation at  $2 < z < 6$ . To minimize the effect of cosmic variance, the targets are selected in three independent extragalactic fields: COSMOS (Scoville et al. 2007), the CFHTLS-D1 Field (Cuillandre et al. 2012) and the Extended-Chandra-Deep-Field (ECDFS; e.g., see Cardamone et al. 2010). The survey is fully presented in Le Fèvre et al. (2014).

### 2.1. Photometry

The three extragalactic fields targeted by the VUDS survey are three of the most studied regions of the sky, and they have been imaged by some of the most powerful telescopes on earth and in the space, including CFHT, Subaru, HST, and *Spitzer*. For more details, we refer the reader to Le Fèvre et al. (2014), where more detailed information can be found.

The COSMOS field was observed with HST/ACS in the *F814W* filter (Koekemoer et al. 2007). Ground based imaging includes deep observations in  $g'$ ,  $r'$ ,  $i'$  and  $z'$  bands from the Subaru SuprimeCam (Taniguchi et al. 2007) and  $u^*$  band observations from CFHT Megacam from the CFHT-Legacy Survey. Moreover, the UltraVista survey is acquiring very deep near-infrared imaging in the  $Y$ ,  $J$ ,  $H$  and  $K$  bands using the VIRCAM camera on the VISTA telescope (McCracken et al. 2012), and deep *Spitzer*/IRAC observations are available (Sanders et al. 2007; Capak et al., in prep.). The CANDELS survey (Grogin et al. 2011; Koekemoer et al. 2011) also provided WFC3 NIR photometry in the *F125W* and *F160W* bands, for the central part of the COSMOS field.

The ECDFS field is covered with deep UBVRI imaging down to  $R_{AB} = 25.3$  ( $5\sigma$ , Cardamone et al. 2010 and references therein). For the central part of the field, covering  $\sim 160$  arcmin<sup>2</sup>, observations with HST/ACS in the *F435W*, *F606W*, *F775W* and *F850LP* are available (Giavalisco et al. 2004), together with the recent CANDELS observations in the  $J$ ,  $H$  and  $K$  bands. The SERVS *Spitzer*-warm obtained  $3.6 \mu\text{m}$  and  $4.5 \mu\text{m}$  (Mauduit et al. 2012) that complement those obtained by the GOODS team at  $3.6 \mu\text{m}$ ,  $4.5 \mu\text{m}$ ,  $5.6 \mu\text{m}$  and  $8.0 \mu\text{m}$ .

The VVDS-02h field is observed in the BVRI at the CFHT (Le Fèvre et al. 2004), and later received deeper observations in the  $u^*$ ,  $g'$ ,  $r'$  and  $i'$  bands as part of the CFHTLS survey (Cuillandre et al. 2012). Deep infrared imaging has been obtained with the WIRCAM at CFHT in  $YJHK$  bands down to  $K_s = 24.8$  (Bielby et al. 2012). This field was observed in all *Spitzer* bands as part of the SWIRE survey (Lonsdale et al. 2003), and recently deeper data were obtained as part of the SERVS survey (Mauduit et al. 2012).

### 2.2. Target selection

The aim of the VUDS survey is to build a well controlled and complete spectroscopic sample of galaxies in the redshift range

$2 \lesssim z \lesssim 6$ . To achieve this goal, with the aim of being as inclusive as possible, we combined different selection criteria such as photometric redshifts, color-color and narrow-band selections. All the details of the selection can be found in Le Fèvre et al. (2014).

For this paper, we limited the analysis to the objects selected by the primary selection, that is based on photometric redshift and magnitude in the  $i'$ -band. In particular, only galaxies with auto magnitude in the  $i'$ -band  $22.5 < m_i < 25$  are included. If an object has a photometric redshift  $z_p > 2.4 - \sigma_{z_p}$  (where  $\sigma_{z_p}$  denotes the  $1-\sigma$  error on the photometric redshift) or if the second peak of the photometric redshift Probability Distribution Function (zPDF)  $z_{p,2} > 2.4$ , this object is included in the target list.

### 2.3. Spectroscopy

The spectroscopic observations were carried out with the VIMOS instrument on the VLT. A total of 640h were allocated, including overheads, starting in periods P85 and ending in P93 (end of 2013) to observe a total of 16 VIMOS pointings. The spectroscopic MOS masks were designed using the *vmmops* tool (Bottini et al. 2005) to maximize the number of spectroscopic targets that could be placed in them. In the end, around 150 targets were placed in each of the 4 VIMOS quadrants, corresponding to about 600 targets per pointing and about 9000 targets in the whole survey. The same spectroscopic mask was observed once for 14 h with the LRBLUE grism ( $R = 180$ ) and for 14 h with the LRRED grism ( $R = 210$ ), resulting in a continuous spectral coverage between  $\lambda = 3650 \text{ \AA}$  and  $\lambda = 9350 \text{ \AA}$ . Le Fèvre et al. (2014) used the data from the VVDS survey to estimate the redshift accuracy of this configuration, constraining it to  $\sigma_{z_{\text{spec}}} = 0.0005(1 + z_{\text{spec}})$ , which corresponds to  $\sim 150 \text{ km s}^{-1}$ .

The spectroscopic observations are reduced using the VIPGI code (Scodreggio et al. 2005). First, the individual 2D spectrograms coming from the 13 observing batches (OBs), in which the observations are splitted, are extracted. Sky subtraction is performed with a low order spline fit along the slit at each wavelength sampled. The sky subtracted 2D spectrograms are combined with sigma clipping to produce a single stacked 2D spectrogram calibrated in wavelength and flux. Then, the objects are identified by collapsing the 2D spectrograms along the dispersion direction. The spectral trace of the target and other detected objects in a given slit are linked to the astrometric frame to identify the corresponding target in the parent photometric catalogue. At the end of this process 1D sky-corrected, stacked and calibrated spectra are extracted. For more detail, we refer the reader to Le Fèvre et al. (2014).

The redshift determination procedure follows the one that was optimized for the VVDS survey (Le Fèvre et al. 2005), later used in the context of the zCOSMOS survey (Lilly et al. 2007) and VIPERS (Guzzo et al. 2014): each spectrum is analyzed by two different team members; the two independent measurements are then reconciled and a final redshift with a quality flag are assigned. The EZ tool (Garilli et al. 2010), a cross-correlation engine to compare spectra and a wide library of galaxy and star templates, is run on all objects to obtain a first guess of the redshift; after a visual inspection of the solutions, it is run in manual mode to refine them, if necessary.

A quality flag is assigned to each redshift, repeating the same scheme already used for the VVDS, COSMOS and VIPERS survey. The flag scheme was thoroughly tested in the context of the VVDS survey, on spectra of similar quality than the one we

have for VUDS, and it is remarkably stable, since the individual differences are smoothed out by the process that involves many people (Le Fèvre et al. 2014). In particular, Le Fèvre et al. (2014) estimated the reliability of each class:

- Flag 4: 100% probability to be correct;
- Flag 3: 95–100% probability to be correct;
- Flag 2: 75–85% probability to be correct;
- Flag 1: 50–75% probability to be correct;
- Flag 0: no redshift could be assigned;
- Flag 9: the spectrum has a single emission line.

The equivalent width (EW) of the Ly $\alpha$  line was measured manually using the *plot* tool in the *noao.onedspec* package in IRAF, similarly to Tresse et al. (1999). We first put each galaxy spectrum in its rest-frame according to the spectroscopic redshift. Then, two continuum points bracketing the Ly $\alpha$  are manually marked and the rest-frame equivalent width is measured. The line is not fitted with a Gaussian, but the flux in the line is obtained integrating the area encompassed by the line and the continuum. This method allows the measurement of lines with asymmetric shapes (i.e., with deviations from Gaussian profiles), which is expected to be the case for most Ly $\alpha$  lines. The interactive method also allows us to control by eye the level of the continuum, taking into account defects that may be present around the line measured. It does not have the objectivity of automatic measurements, but, given the sometimes complex blend between Ly $\alpha$  emission and Ly $\alpha$  absorption, it does produce reliable and accurate measurements. We stress here that the  $m_i < 25$  selection ensures that the continuum around Ly $\alpha$  is well detected for all galaxies in our sample, even for galaxies with spectroscopic flag 1 (the lowest quality) and 9 (objects with a single emission line).

We report in Fig. 1 six examples of spectra in our sample. These objects are representative of the range of magnitudes, redshifts and Ly $\alpha$  EW covered by the sample. We note that the fit to the continuum shown in the examples is not used at all for the scientific analysis presented in this paper. It is only shown as a guide to select the continuum points bracketing the Ly $\alpha$  line. For some more examples of spectra used in this study, we refer the reader to Le Fèvre et al. (2014).

#### 2.4. Absolute magnitudes and masses

We fitted the spectral energy distributions of galaxies in the survey using the Le Phare tool (Ilbert et al. 2006), following the same procedure described in Ilbert et al. (2013). The redshift is fixed to the spectroscopic one for objects with flags 1, 2, 3, 4 and 9. It is fixed to the photometric one for objects with spectroscopic flag 0. In particular, we used the suite of templates by Bruzual & Charlot (2003) with 3 metallicities ( $Z = 0.004, 0.008, 0.02$ ), assuming the Calzetti et al. (2000) extinction curve. We used exponentially declining star formation histories, with nine possible  $\tau$  values ranging from 0.1 Gyr (almost instantaneous burst) to 30 Gyr (smooth and continuous star formation). Moreover, since there is now growing evidence that exponentially increasing models can better describe the SFH of some galaxies beyond  $z = 2$  (Maraston et al. 2010; Papovich et al. 2011; Reddy et al. 2012), we also included two delayed SFH models, for which  $SFR \propto \tau^{-2}te^{-t/\tau}$ , with  $\tau$  that can be 1 or 3 Gyr. For all models, the age ranges 0.05 Gyr and the age of the Universe at the reshift of each galaxy. Since all galaxies in our sample have  $z > 2$ , and the Universe was already 3 Gyr old at that redshift, all the galaxies in our sample fitted with the delayed SFH with  $\tau = 3$  Gyr are caught when the SFH is rising. In

the end, we let the fitting procedure decide what the best model is for each galaxy, if increasing or declining.

For each synthetic SED, emission lines are added to the synthetic spectra, with their luminosity set by the intensity of the SFR. Once the H $\alpha$  luminosity is obtained from the SFR applying the classical Kennicutt (1998) relations, the theoretical Ly $\alpha$  luminosity is obtained assuming case B recombination (Brocklehurst 1971). Then, the actual Ly $\alpha$  luminosity that is added to the SED is allowed to vary between half and double the theoretical value. The absolute magnitudes are then derived by convolving the best template with the filter responses. The output of this fitting procedure also includes the stellar masses, star formation rates and extinction  $E(B - V)$ .

#### 2.5. The dataset

For this paper we limit the analysis to the redshift range  $2 < z < 6$ . The lower limit is the lowest redshift for which the Ly $\alpha$  line is redshifted into our spectral coverage. For the upper limit, in theory, we could detect Ly $\alpha$  in emission up to  $z \sim 6.5$ , but the scarcity of objects at  $z > 6$  in the VUDS survey forced us to limit the analysis to  $z \sim 6$ . We limit the analysis to the galaxies with  $m_i < 25$ : at these magnitudes the continuum is always detected with signal-to-noise ratio per resolution element  $S/N \sim 10$ , ensuring that UV emission and absorption lines with intrinsic  $|EW| \gtrsim 2$  are easily identified in the spectra and the redshift determination is quite reliable, for both spectra with Ly $\alpha$  in emission and absorption. As we already said in the Introduction, the Ly $\alpha$  line enters the  $i'$ -band only at  $z > 5$ : this ensures that no detection bias affects our analysis at  $z < 5$ . We have in our sample only 12 galaxies at  $5 < z < 6$ : we choose to keep them for our analysis throughout the paper, but we will be extremely cautious to draw strong conclusions for that redshift range.

We also include in the analysis secondary objects, that is the objects that serendipitously fall in the spectroscopic slit centered on a target, for which a spectrum is obtained in addition to that of the target. For these objects, if they are brighter than  $m_i < 25$ , a spectroscopic redshift can also be easily assigned. However, only 2% of the final sample is made by secondary objects, that in any case only marginally affect the main result of this paper. The database contain 4420 objects with  $m_i < 25$  that have been targeted by spectroscopy. Of these, 3129 have a high reliability spectroscopic redshift in the range  $2 < z < 6$ , with a spectroscopic flag 2, 3 or 4. Of the remaining objects, 1058 have a more uncertain spectroscopic redshift, with a quality flag 1: statistically, Le Fèvre et al. (2014) showed that they are right in 50–75% of the cases. For the purpose of this paper, we decided to trust their spectroscopic redshift if the difference between the photometric and spectroscopic redshift is smaller than 10%; otherwise, we fix the redshift to the photometric one. We stress that almost all of the 1058 objects do not show any strong emission line in their spectra that could be interpreted as Ly $\alpha$ , and that could help to assign a reliable spectroscopic redshift. Thus, they will not be part of the sample of strong Ly $\alpha$  emitters, but they will contribute to the total sample of galaxies without Ly $\alpha$  emission, hence setting a lower limit to the Ly $\alpha$  fraction (see below). In the end, only 601 of these 1058 objects with spectroscopic flag 1 survive the check against the photometric redshift (~60%, not far from the 50–75% determined by Le Fèvre et al. (2014)); the other 459 have a photometric redshift that is below  $z = 2$  and are excluded by the dataset.

In the end we include in our final database 3730 objects with  $m_i < 25$  for which we have measured a redshift and assigned a spectroscopic flag from 1 to 9. Of them, 3650 are

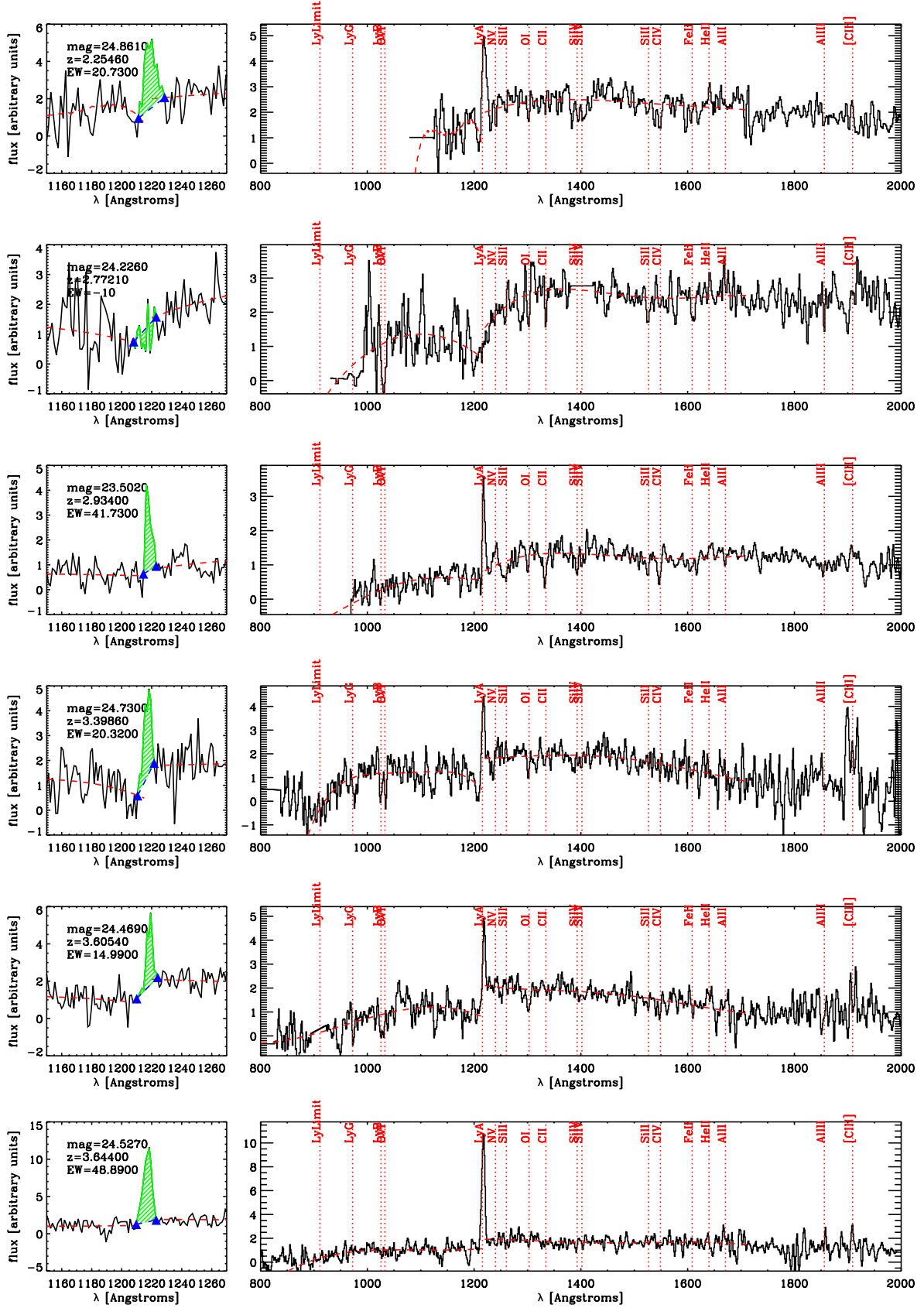


**Fig. 1.** Six examples of spectra for the galaxies in the sample. The *left panels* show the region around Ly $\alpha$ , while the *right ones* show the full spectrum, with the most common UV rest-frame lines highlighted in red. These examples are chosen to be representative of the *i*-band magnitudes, redshifts and Ly $\alpha$  equivalent widths covered by the sample presented in this work. The red dashed curves show polynomial fits to the continuum: for each spectrum, the region between 912 Å and Ly $\alpha$  and the region between Ly $\alpha$  and 2000 Å are fitted separately. We note that the fits are not used at all in the analysis presented in this paper; they only provide a guidance to assess the continuum around Ly $\alpha$ . The blue triangles show the points on the continuum bracketing the Ly $\alpha$  line, shown in green.

**Table 1.** The final sample of galaxies used in this work, divided in 4 redshift bins, as a function of the spectroscopic quality flag.

	$2 < z < 2.7$	$2.7 < z < 3.5$	$3.5 < z < 4.5$	$4.5 < z < 6$
$f = 0$	83(0)	90(0)	40(0)	18(0)
$f = 1$	299(2)	200(3)	88(2)	14(0)
$f = 2$	614(24)	614(17)	163(5)	47(3)
$f = 3, 4$	646(106)	701(153)	205(57)	41(22)
$f = 9$	28(15)	31(10)	19(6)	20(5)

**Notes.** The number in parentheses indicates the number of objects at that redshift and of that spectroscopic quality flag that have  $EW_0 > 25 \text{ \AA}$ .

primary targets, and in addition we have 80 secondary objects with  $m_i < 25$ . Moreover, 231 objects with a photometric redshift in the range  $2 < z < 6$  and  $m_i < 25$  have been targeted by spectroscopy, but no spectroscopic redshift could be measured (they are identified by the spectroscopic flag = 0). In the next sections, we will take into account their possible contribution to the evolution of the fraction of the Ly $\alpha$  emitters.

In order to allow a fair comparison with other works in the literature, we define as strong Ly $\alpha$  emitters all the galaxies with a rest-frame equivalent width of Ly $\alpha$  in excess of 25  $\text{\AA}$ . In the end, 430 of the 3961 galaxies ( $\sim 11\%$ ) meet this definition.

The details about the number of objects for each flag class, as a function of the presence of strong Ly $\alpha$  emission, can be found in Table 1. The large majority of the galaxies used in this study has a spectroscopic redshift with very high reliability: in fact, 1438 objects (36% of the total) have a spectroscopic flag 2, meaning that they are right in 75–85% of the cases (Le Fèvre et al. 2014); 1593 objects (42% of the total) have a spectroscopic flag 3 or 4, that are proven to be right in more than 95% of the cases, 601 (15% of the total) are the objects with spectroscopic quality 1, but for which the spectro- $z$  differs less than 10% from the photometric one and 98 objects ( $\sim 2\%$  of the total) have a spectroscopic flag 9, meaning that only one feature, in their case Ly $\alpha$ , has been identified in the spectrum, and for which about 80% are proven to be right (Le Fèvre et al. 2014). Finally, 231 objects ( $\sim 6\%$  of the total) have spectroscopic flag 0, meaning that a spectroscopic redshift could not be assigned.

From Table 1, it is evident that the vast majority of objects with strong Ly $\alpha$  ( $EW_0 > 25 \text{ \AA}$ ) have been assigned a quality flag of 3 or 4: this is not surprising, and it reflects a tendency by the redshift measurers to assign an higher flag when the spectrum has Ly $\alpha$  in emission. We note as well that not all the galaxies with flag 9 are strong Ly $\alpha$  emitters, although all of them, of course, have Ly $\alpha$  in emission (it is the only spectral feature identified in their spectrum): only in  $\sim 40\%$  of the cases is the emission strong enough to pass the equivalent width threshold of 25  $\text{\AA}$ .

We show in Fig. 2 the absolute magnitude in the far-UV as a function of redshift for the 3730 galaxies in the selected sample. We compare the distribution of our galaxies with the evolution of  $M_{\text{FUV}}^*$  as derived by fitting the values for  $M_{\text{FUV}}^*$  compiled by Hathi et al. (2010). In more detail, Hathi et al. (2010) derive the  $F_{\text{UV}}$  luminosity function of star-forming galaxies at  $z \sim 2$ –3, constraining its slope and characteristic magnitude, and compare their values with other in the literature between  $z \sim 0$  and  $z \sim 8$ . With the aim of deriving an evolving  $M_{\text{FUV}}^*$  as a function of the redshift, we took the values published by Arnouts et al. (2005) at  $0 < z < 3$ , Hathi et al. (2010) at  $2 < z < 3$ , Reddy & Steidel (2009) at  $z \sim 3$ , Ly et al. (2009) at  $z \sim 2$ , Bouwens et al. (2007)

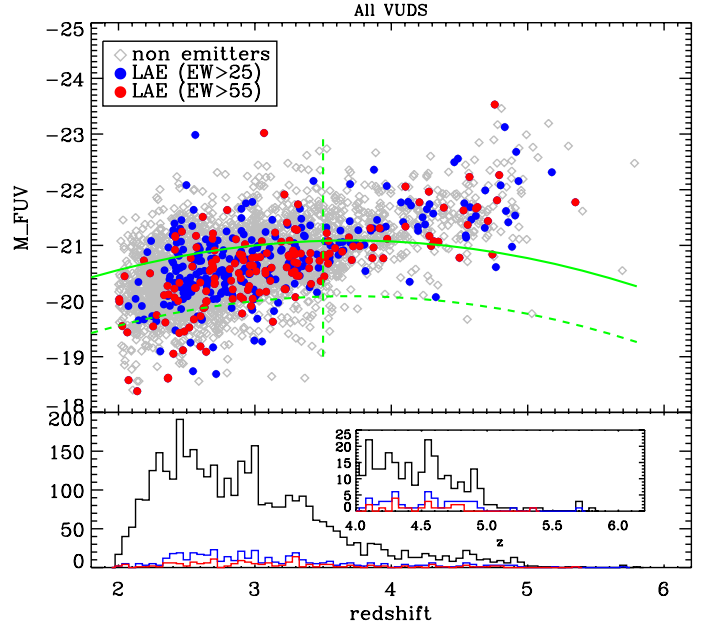


**Fig. 2.** Top panel: absolute magnitude in the far-UV band as a function of the redshift, for all VUDS galaxies at  $2 < z < 6$  (gray diamonds), for the galaxies with  $EW_0 > 25 \text{ \AA}$  (blue circles) and for the galaxies with  $EW_0 > 55 \text{ \AA}$  (red circles). The green continuous curve indicates the evolving  $M^*$  as a function of the redshift as derived from the compilation by Hathi et al. (2010); the dashed green curve indicates  $M^* + 1$ . The vertical dashed line shows  $z = 3.5$ , the redshift up to which the faint sample is complete. Bottom panel: redshift distribution of the all the VUDS galaxies at  $2 < z < 6$  (black line) and of the VUDS galaxies with  $EW_0 > 25 \text{ \AA}$  (blue histogram) and  $EW_0 > 55 \text{ \AA}$  (red histogram).

at  $z \sim 4, 5, 6$ , Sawicki et al. (2006) at  $z \sim 4$  and Mc Lure et al. (2009) at  $z \sim 5, 6$  and we fitted a parabola to them. In particular, we get this best-fit:

$$M^*(z) = -18.56 - 1.37 \times z + 0.18 \times z^2. \quad (1)$$

We report this best fit on Fig. 2, together with the curve corresponding to  $M_{\text{FUV}}^* + 1$ : we can see that the data sample quite well the far-UV luminosities brighter than  $M^*$  up to redshift  $z \sim 5$ . Similarly, we probe the luminosity down to one magnitude fainter than  $M_{\text{FUV}}^*$  up to redshift  $z \sim 3.5$ . We also note that at  $z > 5$ , where the Ly $\alpha$  line and the Ly $\alpha$  forest absorptions by the IGM enter the  $i'$ -band, we only detect the brightest UV galaxies, while we completely miss galaxies around  $M_{\text{FUV}}^*$ . In the remaining of the paper, we will be cautious to include galaxies at  $z > 5$  in our analysis, and where we will do so, we will discuss the consequences.

For the analysis that we present in the following sections we build two volume limited samples: the bright one, that contains all galaxies brighter than  $M_{\text{FUV}}^*$  at redshift  $2 < z < 6$ ; and the faint one, that contains galaxies with  $M_{\text{FUV}} < M_{\text{FUV}}^* < M_{\text{FUV}} + 1$ , limited at  $z < 3.5$ . This approach is slightly different than the one used in similar studies in the literature: Stark et al. (2010, 2011) and Mallery et al. (2012), for example, rather use fixed intervals of absolute magnitudes at all redshift. However, we prefer here to account for the evolution of the characteristic luminosity of star-forming galaxies, comparing at different redshifts galaxies that are in the same evolutionary state.

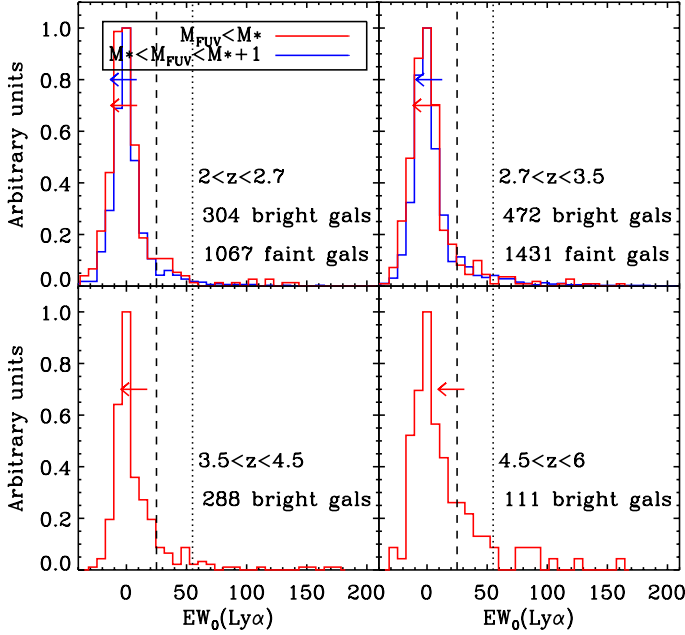


**Fig. 3.** Rest-frame equivalent width  $EW_0$  of the Ly $\alpha$  line in four redshift bins. The dashed and dotted lines, respectively at  $EW_0 = 25$  and  $55$  Å, represent the two thresholds that we apply in the analysis. The red and blue histogram indicate the bright sample ( $M_{\text{FUV}} < M^*$ ) and the faint ( $M^* < M_{\text{FUV}} < M^* + 1$ ) one, respectively. 80% of the galaxies in each panel have an  $EW_0(\text{Ly}\alpha)$  below the value indicated by the arrow.

### 3. The distribution of the rest-frame EW of Ly $\alpha$

We show in Fig. 3 the distribution of the rest-frame EW of Ly $\alpha$  in four redshift bins, for the bright and faint samples separately. Positive EW indicate that Ly $\alpha$  is in emission, and negative EW indicate that the line is in absorption.

Although we measured the equivalent width of Ly $\alpha$  for all the 3730 objects with a measured spectroscopic redshift (all the galaxies with spectroscopic flag 2, 3, 4 and 9, and also the objects with flag 1 for which the spectroscopic redshift differs less than 10% from the photometric one), this figure includes only the 3204 objects in the bright and faint volume limited samples. These are the largest volume limited samples of UV selected galaxies with almost full spectroscopic information ever collected in the literature, and they allow us to constrain the EW distribution of the Ly $\alpha$  line from star-forming objects with strong Ly $\alpha$  in absorption compared to those with strong Ly $\alpha$  in emission. It can be seen that the shape of the distribution is similar at all redshifts: it is lognormal and it extends from  $-50$  Å to  $200$  Å, with the peak at  $EW_0 = 0$  at all redshift and for all luminosities.

In the first two redshift bins,  $2 < z < 2.7$  and  $2.7 < z < 3.5$ , we can compare the EW distributions of the bright and faint sample, and we can see that they are quite similar. However, the extension of the tail of objects with large  $EW_0(\text{Ly}\alpha)$  evolves fast with redshift: while at  $2 < z < 2.7$  11% (7%) of the bright (faint) galaxies have  $EW_0(\text{Ly}\alpha) > 25$  Å, that fraction increases to  $\sim 15\%$  (12%) at  $2.7 < z < 4$  and to 25% at  $z \sim 5$ . Similarly, we observe an evolution with redshift of the upper  $EW_0(\text{Ly}\alpha)$  threshold which contains 80% of the sources: at  $2 < z < 3.5$  the threshold is around  $10$ – $12$  Å (for galaxies in both the bright and faint samples), at  $3.5 < z < 4.5$  it evolves to  $\sim 18$  Å and at  $4.5 < z < 6$  it moves to  $\sim 30$  Å.

We note as well that the only 13 galaxies in the whole sample have  $EW_0 > 150$  Å (the highest value is  $EW_0 = 278.2$  at  $z = 2.5661$ ). So extreme  $EW_0(\text{Ly}\alpha)$  can not be easily produced by star formation with a Salpeter IMF, but must have a top-heavy IMF, a very young age  $< 10^7$  yr and/or a very low metallicity (Schaerer 2003).

### 4. The evolution of the fraction of strong Ly $\alpha$ emitters among star-forming galaxies at $2 < z < 6$

We present in Fig. 4 the evolution with the redshift of the fraction of star-forming galaxies that have an equivalent width of  $EW_0(\text{Ly}\alpha) > 25$  Å (left panel) and  $EW_0(\text{Ly}\alpha) > 55$  Å (right panel), for the bright sample ( $M_{\text{FUV}} < M^*$ ) and for the faint one ( $M^* < M_{\text{FUV}} < M^* + 1$ ) separately. In both panels we show the same fraction for galaxies with  $-21.75 < m_{\text{FUV}} < -20.25$ , for consistency with previous studies (Stark et al. 2010, 2011; Mallery et al. 2012). As we showed in Fig. 2, while the bright sample ( $M_{\text{FUV}} < M^*$ ) is well represented up to  $z \sim 6$ , the faint one is represented only up to  $z \sim 3.5$ : in fact, the cut in observed magnitude at  $m_i < 25$ , that we apply to be sure that the continuum is detected in spectroscopy with a S/N high enough to detect possible UV absorption features, basically prevents us by construction from having faint galaxies in our sample beyond  $z \sim 3.5$ .

Our fiducial case is obtained when we include all objects with spectroscopic flag 2, 3, 4 and 9, and we also add the “good” flag 1 (those objects for which the spectroscopic and photometric redshifts differ by less than 10%) to the distribution. However, it is possible that this combination slightly overestimates the true fraction, as we know that 231 objects with photometric redshift  $2 < z < 6$  have been observed in spectroscopy, but for them a spectroscopic redshift could not be assigned. So, it is possible that a fraction of them are actually at  $2 < z < 6$ , and since no Ly $\alpha$  is present in the whole observed spectral range, they will decrease the fraction of strong Ly $\alpha$  emitters by a given amount. We discuss in Fig. 5 the effect on the fraction of emitters of the choice of including objects with spectroscopic flag 0 and 1, that is quite minimal.

In Fig. 4, for the three ranges of UV luminosities, we also show the fractions obtained on a finer redshift grid ( $\Delta z \sim 0.3$ ) and on a coarser grid, that highlights the general trend and smooth out variations due to cosmic variance. The fine grid extends on the whole  $2 < z < 6$  range for the bright sample: however, only the highest redshift bin contains galaxies at  $5 < z < 6$  and might be affected by the detection bias due to the Ly $\alpha$  line entering the  $i'$ -band at that redshift. In the case of the coarser grid we limited the analysis to the galaxies at  $z < 5$ , so to be sure that the results are not dependent on that effect.

For the bright sample, the evolution of the fraction of emitters with  $EW_0(\text{Ly}\alpha) > 25$  Å, shown in the left panel of Fig. 4, is characterized by a very modest increase in the fraction of Ly $\alpha$  emitters between redshift  $z \sim 2$  and  $z \sim 4$  (from  $\sim 10\%$  at  $z \sim 2$  to  $\sim 15\%$  at  $z \sim 4$ ), and then by a faster increase above  $z \sim 4$  (the fraction reaches  $\sim 25\%$  at  $z \sim 5$  and  $\sim 30\%$  at  $z \sim 5.5$ ). A very similar trend is observed when galaxies with  $-21.75 < m_{\text{FUV}} < -20.25$  are considered. If we then analyze the faint sample, and we compare it with the bright one, we find that the overall fraction of objects with  $EW_0(\text{Ly}\alpha) > 25$  Å (or  $EW_0(\text{Ly}\alpha) > 55$  Å) is similar to that of the bright sample between  $z \sim 2$  and  $z \sim 3.5$ , but the evolution between  $z \sim 2.3$  and  $z \sim 3$  is much faster for the faint sample. This is in apparent disagreement with the results

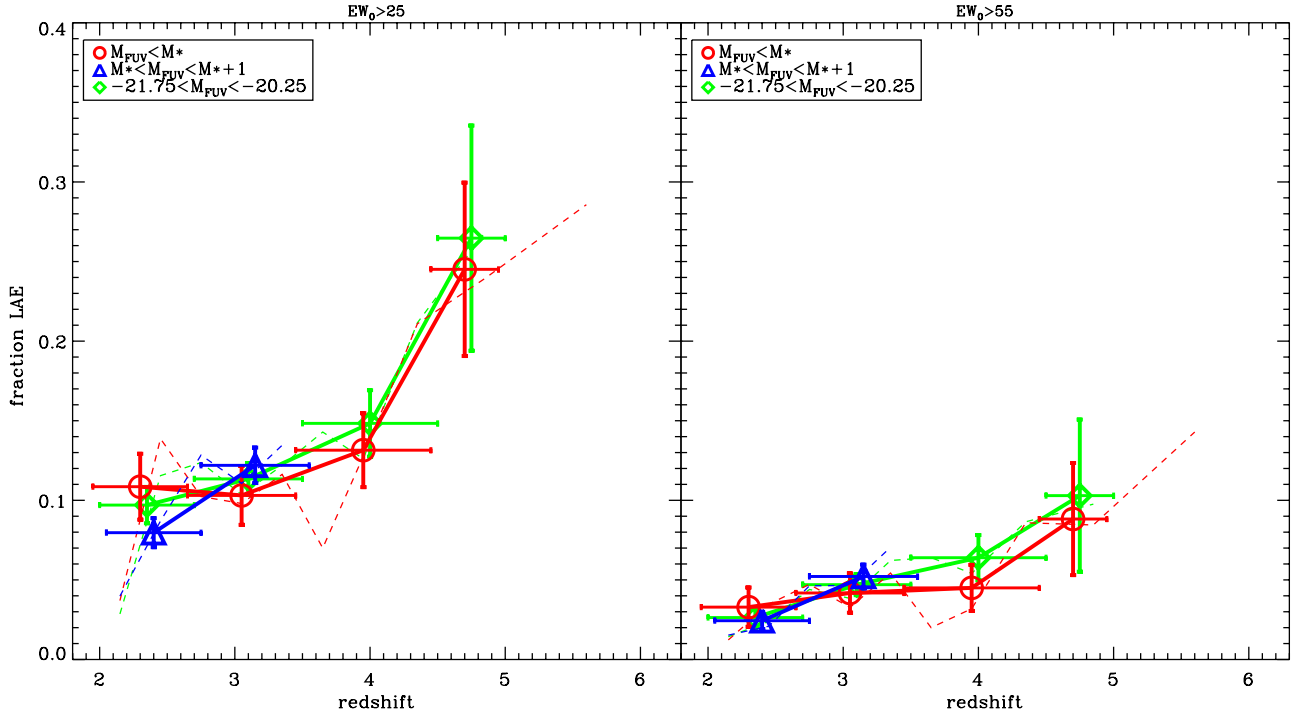


**Fig. 4.** *Left panel:* our best estimate of the fraction of galaxies with  $EW_0(\text{Ly}\alpha) > 25 \text{ \AA}$ , as a function of the redshift, for three intervals of far-UV absolute magnitudes: faint objects ( $M^* < M_{\text{FUV}} < M^* + 1$ ) are shown in blue; bright objects ( $M_{\text{FUV}} < M^*$ ) are shown in red; objects with  $-21.75 < M_{\text{FUV}} < -20.25$  are shown in green. The fiducial values, shown by the continuous thick lines, include all the galaxies with spectroscopic flag 2, 3, 4 and 9, and also all the galaxies with a spectroscopic redshift that differs less than 10% from the photometric one. The dashed lighter lines show a finer binning in redshift. *Right panel:* same as *left panel*, but for galaxies with  $EW_0(\text{Ly}\alpha) > 55 \text{ \AA}$ .

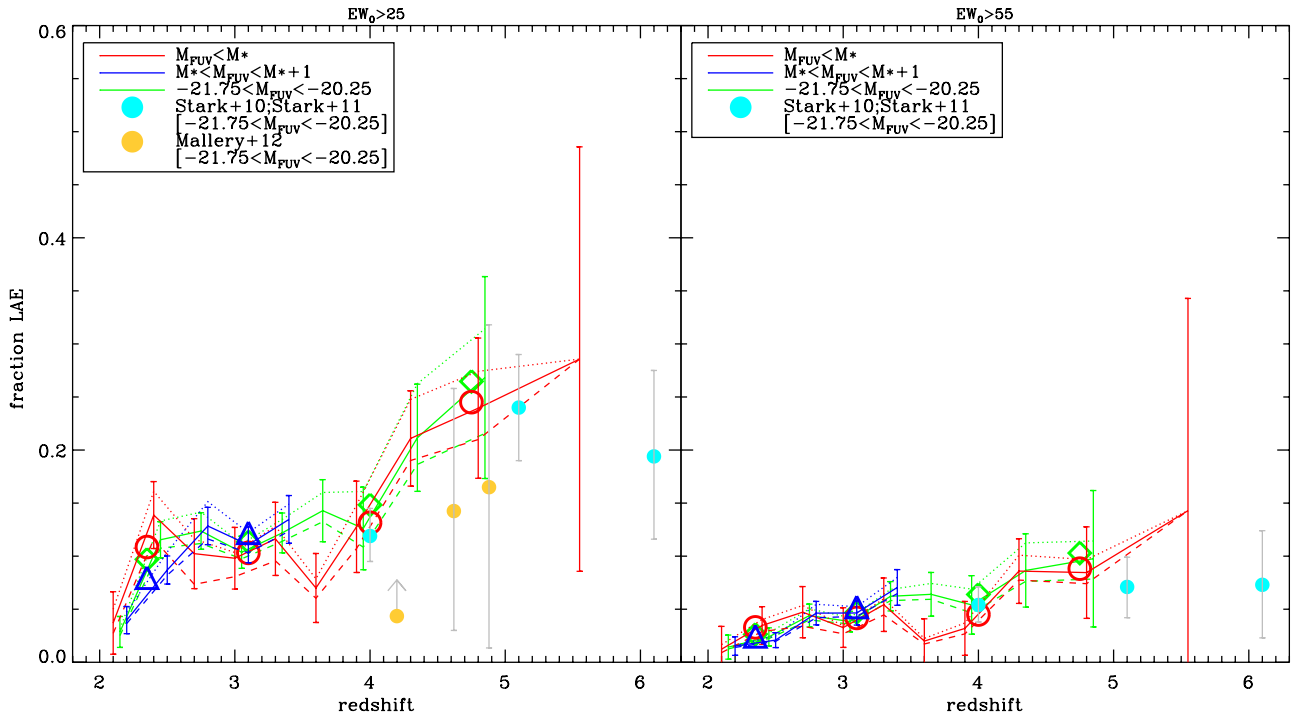


**Fig. 5.** Same as Fig. 4, but with a finer binning in redshift, and showing the effect of including galaxies with flags 0 and 1. The *left panel* shows the case when the galaxies with  $EW_0(\text{Ly}\alpha) > 25 \text{ \AA}$  are considered as emitters, and the *right panel* when the threshold is fixed at  $EW_0(\text{Ly}\alpha) > 55 \text{ \AA}$ . The fiducial values, shown by the continuous thick lines, include all the galaxies with spectroscopic flag 2, 3, 4 and 9, and also all the galaxies with a spectroscopic flag 1 and a spectroscopic redshift that differs less than 10% from the photometric one. The dotted line shows the case when only flags 2, 3, 4, and 9 are considered; the dashed line is the same as the fiducial case, but the galaxies with no spectroscopic redshift (flag = 0) are also included, with the redshift fixed to the photometric one. The red curves are for the bright volume limited sample; the blue ones are for the faint one; the green ones are for galaxies with  $-21.75 < m_{\text{FUV}} < -20.25$ . For clarity, the error bars are shown only for the continuous curves. The cyan points are from Stark et al. (2010, 2011), the yellow ones from Mallery et al. (2012). The red circles, blue triangles and green lozenges show the coarser binning in redshift adopted in Fig. 4.

by Stark et al. (2010, 2011), who found both a higher fraction of Ly $\alpha$  emitters and a steeper evolution of this fraction among faint UV galaxies ( $-20.25 < M_{\text{FUV}} < -18.75$ ) than among bright UV galaxies ( $-21.75 < M_{\text{FUV}} < -20.25$ ). However, we note that the range of UV luminosities probed by our study is narrower than the one probed by Stark et al. (2010, 2011).

The right panel of Fig. 4 shows the effect on the fraction of Ly $\alpha$  emitters of changing the EW threshold from 25 Å to 55 Å. It can be seen that, as expected, the fraction drastically decreases at all redshifts. However, the general trend observed in the left panel of Fig. 4 is preserved: we observe that the fraction remains around 3–4% with a slight increase in  $2 < z < 4$ , then it increases faster between  $z \sim 4$  and  $z \sim 5$  rising from 5% to 12%.

An important point that needs to be stressed again here is that our selection criteria are completely independent of the presence and strength of the Ly $\alpha$  emission up to  $z \sim 5$ . This selection ensures that there are no biases in the determination of this fraction over the range  $2 < z < 5$ : if, for some reason, our selection is less complete in a given redshift range, it will be homogeneously incomplete for galaxies with and without Ly $\alpha$ , and thus the result shown in this section will remain robust.

We report again the evolution of the fraction of Ly $\alpha$  emitters with  $EW_0 > 25$  Å and  $EW_0 > 55$  Å in Fig. 5, where we simply highlight the results on the finer redshift grid and we show the effect of including objects with spectroscopic flag 0 and 1 in the analysis. In this figure, as in Fig. 4, we consider our fiducial case the one including all the “good” flag 1 (objects with a spectroscopic flag 1, for which the spectroscopic redshift and the photometric one differ by less than 10%), together with flags 2, 3, 4, and 9. If objects with spectroscopic flag 1 are excluded, and only flags 2, 3, 4, and 9 are considered, the fraction of emitters increases by  $\sim 2\%$ , with respect to the fiducial value, at all redshifts and for all UV luminosities. This is quite obvious: since basically all the strong Ly $\alpha$  emitters have a spectroscopic flag 2, 3, 4 and 9 (see Table 1), this set of flags maximizes the fraction. On the other hand, if the objects with flag 0 are also considered, together with good flag 1 and all the flags 2, 3, 4, and 9, the fraction decreases by  $\sim 2\%$  with respect to the fiducial case. This effect is also easy to understand: objects with flag 0 are all non-emitters, because if an emission line had been identified they would have been assigned a redshift and a flag, and thus their net effect is to decrease the fraction. Although we can not know for sure how many of these objects with no spectroscopic redshift are indeed at the photometric redshift, their effect is almost negligible: for both Figs. 4 and 5, the effect of considering flags 2, 3, 4, and 9 or of including good flag 1 and flag 0 is always below a few percent.

We also note that our values are in good agreement with those published by Stark et al. (2010, 2011) and that are based on a completely different method that uses LBG technique to photometrically identify high-redshift galaxies (at  $z \sim 4, 5$  and 6) that are then observed in spectroscopy to look for strong Ly $\alpha$  emission. Our values are slightly higher than those by Mallery et al. (2012) although still compatible within the error bars.

## 5. Ly $\alpha$ escape fraction: driver of the Ly $\alpha$ fraction evolution?

The escape fraction of Ly $\alpha$  photons  $f_{\text{esc}}(\text{Ly}\alpha)$  is defined as the fraction of the Ly $\alpha$  photons that are produced within a given galaxy and that actually escape from the galaxy itself. Given the intrinsic resonant nature of the Ly $\alpha$  photons, it is thought to be dependent on the dust content, geometry of the inter-stellar

gas (ISM) and relative kinematics of the ISM and stars. Atek et al. (2014) and Hayes et al. (2014), studying local samples of Ly $\alpha$  emitters, they found a correlation between  $f_{\text{esc}}(\text{Ly}\alpha)$  and  $E(B - V)$ , with the escape fraction being larger on average in galaxies with low dust content. Kornei et al. (2010) and Mallery et al. (2012), although with smaller samples than the one we use here, found a similar correlation at  $z \sim 3$  and at  $3.5 < z < 6$ , respectively.

The Ly $\alpha$  escape fraction is usually determined by comparing the Ly $\alpha$  luminosity with the dust-corrected H $\alpha$  luminosity, once a recombination regime has been chosen. The H $\alpha$  line in fact is not resonant and it is only attenuated by dust. However, for most of the redshift range of this study H $\alpha$  is redshifted even beyond the reach of near-infrared spectrographs.

An alternative method exploits the expected correlations between intrinsic Ly $\alpha$  luminosity, H $\alpha$  luminosity and the SFR of the galaxy. In particular, we assume that

$$f_{\text{esc}}(\text{Ly}\alpha) = L_{\text{Ly}\alpha,\text{obs}}/L_{\text{Ly}\alpha,\text{int}} = \text{SFR}(\text{Ly}\alpha)/\text{SFR}(\text{SED}), \quad (2)$$

where  $L_{\text{Ly}\alpha,\text{obs}}$  and  $L_{\text{Ly}\alpha,\text{int}}$  are the observed and intrinsic Ly $\alpha$  luminosities, respectively;  $\text{SFR}(\text{Ly}\alpha)$  and  $\text{SFR}(\text{SED})$  are the SFR obtained from the observed Ly $\alpha$  luminosity and the total SFR, respectively. Using Kennicutt (1998) prescription to convert  $L_{\text{Ly}\alpha,\text{int}}$  into  $\text{SFR}(\text{Ly}\alpha)$

$$\text{SFR}(\text{Ly}\alpha) = L_{\text{Ly}\alpha} / (1.1 \times 10^{42}), \quad (3)$$

we finally get

$$f_{\text{esc}}(\text{Ly}\alpha) = \text{SFR}(\text{Ly}\alpha)/\text{SFR}(\text{SED}) = \frac{L_{\text{Ly}\alpha}/(1.1 \times 10^{42})}{\text{SFR}_{\text{SED}}}. \quad (4)$$

We note that Eq. (3) assumes the case B recombination regime (Brocklehurst 1971), that predicts an intrinsic ratio  $L_{\text{Ly}\alpha,\text{int}}/L_{\text{H}\alpha,\text{int}} = 8.7$ .

We stress here that the SFR inferred from fitting Bruzual & Charlot (2003) models to the SED of galaxies give only a crude estimate of the star formation rate and of the dust content of galaxies. This is especially true in the redshift regime probed by VUDS, that is so far poorly explored, and for which independent estimates of the SFR from different methods are scarce. However, the SFR inferred from SED fitting are believed to be on average correct within a factor of 3 (Mostek et al. 2012; Utomo et al. 2014), and thus we choose to use these to obtain at least a crude estimation of the Ly $\alpha$  escape fraction.

We plot in Fig. 6 the escape fraction  $f_{\text{esc}}(\text{Ly}\alpha)$  as a function of the redshift and of dust reddening  $E(B - V)$  for the galaxies in the bright and faint volume limited samples together. We tried to separate the two samples, to check for differences among the two them, but we did not find any, so we decided to show them together. For the galaxies with Ly $\alpha$  in absorption (i.e.,  $EW_0(\text{Ly}\alpha) < 0$ , 1628 galaxies) we artificially set  $f_{\text{esc}}(\text{Ly}\alpha)$  to  $10^{-3}$ . For galaxies with  $EW_0(\text{Ly}\alpha) > 0$  (1576 galaxies), the Ly $\alpha$  escape fraction ranges from  $10^{-4}$  to 1. We calculate as well the median escape fraction in bins of redshift, using the same coarse grid used for Fig. 4, and limiting the highest redshift bin to  $z = 5$ , to avoid possible detection biases affecting our selection at higher  $z$ .

It is clear from this figure that at each redshift and for each  $E(B - V)$  the strong Ly $\alpha$  emitters (with  $EW_0(\text{Ly}\alpha) > 25$  Å or  $EW_0(\text{Ly}\alpha) > 55$  Å) are the (rare) galaxies with the highest Ly $\alpha$  escape fraction. In more details, 80% of the galaxies with escape fraction  $f_{\text{esc}}(\text{Ly}\alpha) > 10\%$  have  $EW_0(\text{Ly}\alpha) > 55$  Å, and 70% of the galaxies with  $f_{\text{esc}}(\text{Ly}\alpha) > 3\%$

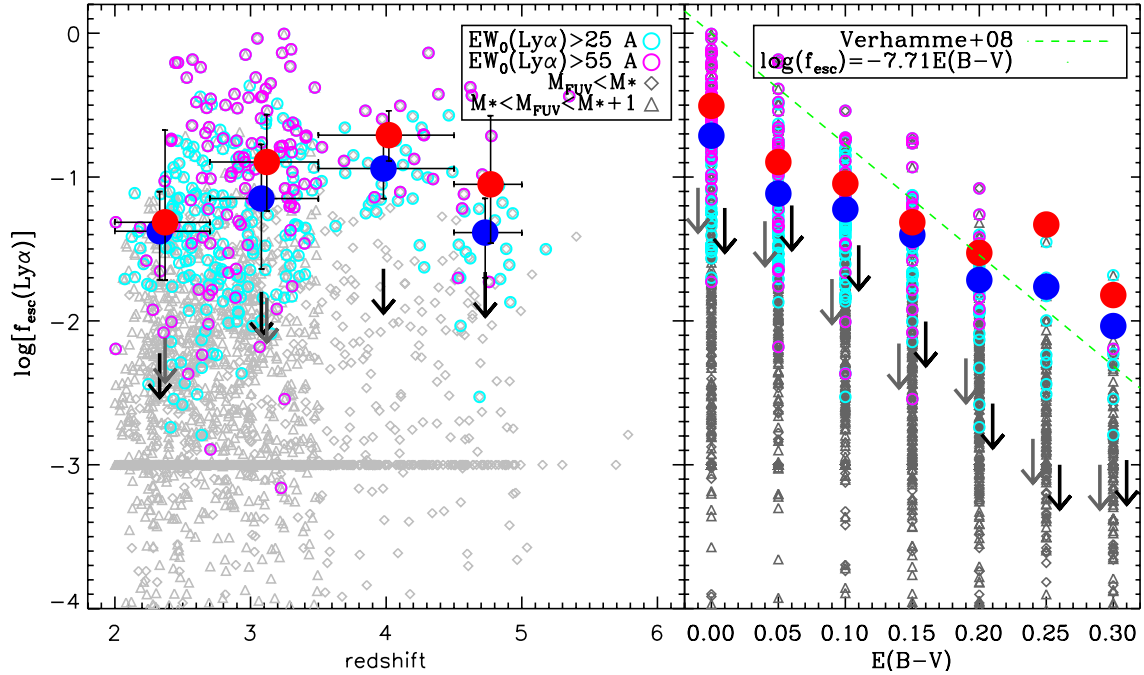


**Fig. 6.** *Left panel:* Ly $\alpha$  escape fraction as a function of redshift for the bright (gray diamonds) and faint (gray triangles) volume limited samples. Strong Ly $\alpha$  emitters with  $EW_0 > 25 \text{ \AA}$  and  $EW_0 > 55 \text{ \AA}$  are shown with cyan and magenta empty circles, respectively. Objects with formally negative equivalent width of Ly $\alpha$ , corresponding to negative Ly $\alpha$  luminosity, are set here to  $\log[f_{\text{esc}}(\text{Ly}\alpha)] = -3$ . The big red and blue circles indicate the median escape fraction for the galaxies with  $EW_0[\text{Ly}\alpha] > 55 \text{ \AA}$  and  $EW_0[\text{Ly}\alpha] > 25 \text{ \AA}$ , respectively. The black (gray) arrows indicate the  $f_{\text{esc}}(\text{Ly}\alpha)$  below which 80% of the bright (faint) objects lie. *Right panel:* Ly $\alpha$  escape fraction as a function of the  $E(B - V)$ . The symbols are the same than in the *left panel*. The green dashed line shows the prediction by Verhamme et al. (2006).

have  $EW_0(\text{Ly}\alpha) > 25 \text{ \AA}$ . The median escape fraction for galaxies  $EW_0(\text{Ly}\alpha) > 25 \text{ \AA}$  is around 8% overall, evolving from 3% at  $z \sim 2.3$  to 8% at  $z \sim 3$  to 12% at  $z \sim 4$ . The median escape fraction for galaxies  $EW_0(\text{Ly}\alpha) > 55 \text{ \AA}$  is of course higher, evolving from 5% at  $z \sim 2.3$  to 12% at  $z \sim 3$  to 20% at  $z \sim 4$ . For both threshold we observe a decrease in the median escape fraction between  $z \sim 4$  and  $z \sim 5$ , which is probably due to the limited amount of data.

If we then consider the whole population in our sample, and we put together the bright and faint volume limited samples, we find that formally the median escape fraction is zero at all redshifts. In fact, the objects with Ly $\alpha$  in absorption (that have  $f_{\text{esc}}(\text{Ly}\alpha)$  fixed to  $10^{-3}$ ) are the majority, at all  $z$ , forcing the median  $f_{\text{esc}}(\text{Ly}\alpha)$  to zero. For this reason, we find more useful to show the evolution of the  $f_{\text{esc}}(\text{Ly}\alpha)$  below which 80% of the galaxies, at each redshift, lie (arrows in Fig. 6). Indeed, this threshold evolves from 1% at  $2 < z < 2.7$  to 1.5% at  $2.7 < z < 3.5$  to 2% at  $3.5 < z < 5$ , with not much difference between the bright and the faint samples.

The comparison of the  $f_{\text{esc}}(\text{Ly}\alpha)$  with the  $E(B - V)$  is also interesting. From the right panel of Fig. 6 we can see that the  $E(B - V)$  anti-correlates with  $f_{\text{esc}}(\text{Ly}\alpha)$ : for objects with high  $E(B - V)$  the median value of  $f_{\text{esc}}(\text{Ly}\alpha)$  is low (and vice versa). This is in qualitative agreement with the results by Hayes et al. (2014) and Atek et al. (2014) in the local Universe, and with Kornei et al. (2010) and Mallery et al. (2012) at high- $z$ . Moreover, the median values for the galaxies with  $EW_0(\text{Ly}\alpha) > 25 \text{ \AA}$  and  $EW_0(\text{Ly}\alpha) > 55 \text{ \AA}$  correlates with the  $E(B - V)$  similarly to the prediction by Verhamme et al. (2006), although our data are better fitted by a flatter slope ( $\sim -5$  in comparison with  $-7.71$  predicted by Verhamme et al. (2006)). However, while galaxies with high  $E(B - V)$  never show large  $f_{\text{esc}}(\text{Ly}\alpha)$ , the contrary is not true: when  $E(B - V)$  is low we observe a broad range

of Ly $\alpha$  escape fractions, ranging from  $10^{-3}$  to 1. This implies that the dust content alone can not be the only factor to regulate  $f_{\text{esc}}(\text{Ly}\alpha)$ , at least for galaxies with the UV luminosities similar to the ones probed in this paper. A possibility is that in these objects Ly $\alpha$  photons are scattered at large distances, instead of being absorbed by dust, similarly to the Ly $\alpha$  haloes presented by Steidel et al. (2011) and Momose et al. (2014). We intend to test this hypothesis by stacking 2d spectra of galaxies with and without Ly $\alpha$  emission in a forthcoming paper.

## 6. Summary, discussion, and conclusions

In this paper we used the unique VUDS dataset to build an unbiased and controlled sample of star-forming galaxies at  $2 < z < 6$ , selected according to the photometric redshifts determined using the overall SED of the galaxies. This selection is complementary to the classical LBG technique, resulting in more complete and less contaminated samples of galaxies at high- $z$ . For the purpose of this paper, even more important is that the combination of the selections we use are independent of the presence of Ly $\alpha$  in emission, at least up to  $z \sim 5$ : whatever incompleteness could affect our sample, it would affect galaxies with and without Ly $\alpha$  in the same way.

The sample is limited at  $m_i < 25$ , ensuring that the continuum is detected with  $S/N \sim 10$  per resolution element: this allows an accurate determination of the spectroscopic redshift through the identification of UV absorption features even for galaxies without Ly $\alpha$  in emission.

We split this sample in two volume limited samples, using a far-UV luminosity cut that is evolving with redshift, following the observed evolution of  $M_{\text{FUV}}^*$  (Hathi et al. 2010): the bright sample include objects that at each redshift are brighter than  $M_{\text{FUV}}^*$ ; the faint one include objects with  $M^* < M_{\text{FUV}} < M^* + 1$ .

We use these two samples to constrain the distribution of the EW of Ly $\alpha$  of star-forming galaxies, that spans from objects with Ly $\alpha$  in absorption to objects with Ly $\alpha$  in emission. We find that  $\sim 80\%$  of the star-forming galaxies in our sample have a Ly $\alpha$  equivalent width  $EW_0(\text{Ly}\alpha) < 15 \text{ \AA}$ .

We use our sample to constrain the evolution of the fraction of strong Ly $\alpha$  emitters among star-forming galaxies at  $2 < z < 6$ . We showed in Sect. 4 that the fraction of strong Ly $\alpha$  emitters with  $EW_0(\text{Ly}\alpha) > 25 \text{ \AA}$  and  $EW_0(\text{Ly}\alpha) > 55 \text{ \AA}$  monotonically increases with redshift, approximately at the same rate for the two EW thresholds. The evolution is characterized by a slower phase between  $z \sim 2$  and  $z \sim 4$ , and by a faster evolution between  $z \sim 4$  and  $z \sim 5.5$ . We see no difference, at  $2 < z < 3.5$  where both samples are well represented, between the fraction of strong emitters in the bright and faint volume limited samples. This is partly in contradiction with results by Stark et al. (2010, 2011), who found that the fraction is higher, and the rate of evolution with redshift faster, for UV faint galaxies at  $4 < z < 6$ . However, this might be due to the narrower range of UV luminosity probed by our work compared to the one probed by Stark et al. (2010, 2011).

Moreover, slicing our sample with the same UV luminosity limits used by Stark ( $-21.75 < M_{\text{FUV}} < -20.25$ ) we see that the evolution of the fraction of strong Ly $\alpha$  emitters (for both  $EW_0(\text{Ly}\alpha) > 25 \text{ \AA}$  and  $EW_0(\text{Ly}\alpha) > 55 \text{ \AA}$ ) is in very good agreement with the values by Stark et al. (2010, 2011), despite the different sample selection methods and available spectroscopy. This is a very important result, placing on firmer grounds the measures of the fraction of star-forming galaxies with Ly $\alpha$  in emission. In fact, their sample is LBG based and only the objects with strong Ly $\alpha$  emission are spectroscopically confirmed. In our case, on the other hand, we stress that all the galaxies, with and without Ly $\alpha$ , have a spectroscopic redshift.

Finally, in Sect. 5, we have explored the possibility that the evolution of the fraction of strong Ly $\alpha$  emitters is primarily due to a change in the escape fraction of Ly $\alpha$  photons. We have found that, as expected, the strong Ly $\alpha$  emitters are the objects for which  $f_{\text{esc}}(\text{Ly}\alpha)$  is the largest. We find as well that the median  $f_{\text{esc}}(\text{Ly}\alpha)$  for the Ly $\alpha$  emitters (with not much difference between objects with  $EW_0(\text{Ly}\alpha) > 25 \text{ \AA}$  and with  $EW_0(\text{Ly}\alpha) > 55 \text{ \AA}$ ) evolves from  $\sim 5\%$  at  $z \sim 2.5$  to  $\sim 20\%$  at  $z \sim 5$ . If we try to estimate the median escape fraction for the whole population, we find that it is formally zero at all redshifts, since the majority of the galaxies in our sample have Ly $\alpha$  in absorption, and  $80\%$  of our galaxies have  $f_{\text{esc}}(\text{Ly}\alpha) < 1\%$ . If we estimate at each redshift the  $f_{\text{esc}}(\text{Ly}\alpha)$  value below which  $80\%$  of the galaxies lie, we find that this value evolves from 1 to 2% between  $z \sim 2$  and  $z \sim 5$ . It is interesting to compare these findings with Hayes et al. (2011), who integrated the Ly $\alpha$  and UV luminosity functions from  $z \sim 0$  to  $z \sim 8$  and then compared the two to estimate the average  $f_{\text{esc}}(\text{Ly}\alpha)$  of the Universe at those redshifts. According to Hayes et al. (2011) the average escape fraction is around 5% at  $z \sim 2$  and 20% at  $z \sim 5$ , values that are much higher than those we obtain for our sample. This implies that for the galaxies with UV luminosities that we sample in this paper ( $M_{\text{FUV}} < M^*$  at  $2 < z < 6$  and  $M^* < M_{\text{FUV}} < M^* + 1$  at  $2 < z < 3.5$ ) the average escape fraction of Ly $\alpha$  photons is much smaller than the average escape fraction of the Universe. In other words, the bulk of the Ly $\alpha$  luminosity, at least in the redshift range  $2 < z < 6$  that is probed in this paper, is not coming from galaxies with the UV luminosities that are probed in this work, but from galaxies that are much fainter in the UV. In fact, Stark et al. (2011) showed that the fraction of strong ( $EW_0(\text{Ly}\alpha) > 25 \text{ \AA}$ ) emitters

is higher in galaxies with  $-20.25 < M_{\text{FUV}} < -18.75$  than in those with  $-21.75 < M_{\text{FUV}} < -20.25$ , implying a larger escape fraction for faint UV galaxies. This is also in line with the results by Ando et al. (2006), who found a deficiency of strong Ly $\alpha$  emitters among UV bright galaxies and by Schaerer et al. (2011), who also found that the fraction of Ly $\alpha$  emitters rapidly increases among galaxies with fainter UV luminosities, indicating that the bulk of the Ly $\alpha$  luminosity in the universe comes from galaxies with  $M_{\text{FUV}} > -20$ .

Similarly to Kornei et al. (2010) and Mallery et al. (2012), we also find that there is an anti-correlation between  $f_{\text{esc}}(\text{Ly}\alpha)$  and the dust content  $E(B - V)$ : galaxies with low  $f_{\text{esc}}(\text{Ly}\alpha)$  have preferentially a higher  $E(B - V)$ , and vice versa. This implies that the dust is a crucial ingredient in setting the escape fraction of galaxies. However, we note that galaxies with low extinction ( $E(B - V) < 0.05$ ) have a very wide range of Ly $\alpha$  escape fractions, ranging from  $10^{-3}$  to 1: this means that the dust content, although important, is not the only ingredient to regulate the fraction of Ly $\alpha$  photons that escape the galaxy. In a forthcoming paper, we will further investigate the dependence of  $f_{\text{esc}}(\text{Ly}\alpha)$  on other quantities as stellar mass, star formation rate and dust content, and on the evolution with redshift of these correlations.

*Acknowledgements.* We thank ESO staff for their continuous support for the VUDS survey, particularly the Paranal staff conducting the observations and Marina Rejkuba and the ESO user support group in Garching. This work is supported by funding from the European Research Council Advanced Grant ERC-2010-AdG-268107-EARLY and by INAF Grants PRIN 2010, PRIN 2012 and PICS 2013. A.C., O.C., M.T. and V.S. acknowledge the grant MIUR PRIN 2010–2011. D.M. gratefully acknowledges LAM hospitality during the initial phases of the project. This work is based on data products made available at the CESAM data center, Laboratoire d’Astrophysique de Marseille. This work partly uses observations obtained with MegaPrime/MegaCam, a joint project of CFHT and CEA/DAPNIA, at the Canada-France-Hawaii Telescope (CFHT) which is operated by the National Research Council (NRC) of Canada, the Institut National des Sciences de l’Univers of the Centre National de la Recherche Scientifique (CNRS) of France, and the University of Hawaii. This work is based in part on data products produced at TERAPIX and the Canadian Astronomy Data Centre as part of the Canada-France-Hawaii Telescope Legacy Survey, a collaborative project of NRC and CNRS.

## References

- Ando, M., Ohta, K., Iwata, I., et al. 2006, *ApJ*, 645, L9  
Atek, H., Kunth, D., Schaerer, D., et al. 2014, *A&A*, 561, A89  
Bielby, R., Hudelot, P., McCracken, H. J., et al. 2012, *A&A*, 545, A23  
Bottini, D., Garilli, B., Maccagni, D., et al. 2005, *PASP*, 117, 996  
Bouwens, R. J., Illingworth, G. D., Franx, M., & Ford, H. 2007, *ApJ*, 670, 928  
Bouwens, R. J., Illingworth, G. D., Franx, M., et al. 2009, *ApJ*, 705, 936  
Bouwens, R. J., Illingworth, G. D., Oesch, P. A., et al. 2010, *ApJ*, 709, L133  
Brocklehurst, M. 1971, *MNRAS*, 153, 471  
Cardamone, C. N., van Dokkum, P. G., Urry, C. M., et al. 2010, *ApJS*, 189, 270  
Caruana, J., Bunker, A. J., Wilkins, S., et al. 2014, *MNRAS*, 443, 2831  
Charlot, S., & Fall, S. M. 1993, *ApJ*, 415, 580  
Cowie, L. L., & Hu, E. M. 1998, *AJ*, 115, 1319  
Cuillandre, J.-C. J., Withington, K., Hudelot, P., et al. 2012, *Observatory Operations: Strategies, Processes and Systems IV*, SPIE, 8448, 84480  
Deharveng, J.-M., Small, T., Barlow, T. A., et al. 2008, *ApJ*, 680, 1072  
Dijkstra, M., & Kramer, R. 2012, *MNRAS*, 424, 1672  
Dijkstra, M., Haiman, Z., & Spaans, M. 2006, *ApJ*, 649, 37  
Dijkstra, M., Wyithe, S., Haiman, Z., et al. 2014, *MNRAS*, 440, 3309  
Djorgovski, S., Spinrad, H., McCarthy, P., & Strauss, M. A. 1985, *ApJ*, 299, L1  
Fontana, A., Vanzella, E., Pentericci, L., et al. 2010, *ApJ*, 725, 205  
Gawiser, E., van Dokkum, P. G., Gronwall, C., et al. 2006, *ApJ*, 642, 13  
Gawiser, E., Harold, F., Kamson, L., et al. 2007, *ApJ*, 671, 278  
Djorgovski, S., Spinrad, H., McCarthy, P., & Calzetti, D. 1996, *ApJ*, 466, 831  
Giavalisco, M., Dickinson, M., Ferguson, H. C., et al. 2004, *ApJ*, 600, 103  
Gronwall, C., Ciardullo, R., Hickey, T., et al. 2007, *ApJ*, 667, 79  
Grogin, N., Kocevski, D. D., Faber, S. M., et al. 2011, *ApJS*, 197, 35  
Guzzo, L., Scoddeggio, M., Garilli, B., et al. 2014, *A&A*, 566, A108  
Hayes, M., Östlin, G., Schaerer, D., et al. 2010, *Nature*, 464, 562

- Hayes, M., Schaerer, D., Östlin, G., et al. 2011, *ApJ*, 730, 8
- Hayes, M., Östlin, G., Duval, F., et al. 2014, *ApJ*, 782, 6
- Hathi, N. P., Ryan, R. E., Jr., Cohen, S. H., et al. 2010, *ApJ*, 720, 1708
- Hathi, N. P., Cohen, S. H., Ryan, R. E., et al. 2013, *ApJ*, 765, 88
- Hu, E. M., Cowie, L. L., Capak, P., et al. 2004, *AJ*, 127, 563
- Kennicutt, R. C., Jr., 1998, *ApJ*, 498, 541
- Koekemoer, A. M., Aussel, H., Calzetti, D., et al. 2007, *ApJS*, 172, 196
- Koekemoer, A. M., Faber, S. M., Ferguson, H. C., et al. 2011, *ApJ*, 197, 36
- Kornei, K. A., Shapley, A. E., Erb, D., et al. 2010, *ApJ*, 711, 693
- Kunth, D., Mas-Hesse, J. M., Terlevich, E., et al. 1998, *A&A*, 334, 11
- Le Fèvre, O., Mellier, Y., McCracken, H. J., et al. 2004, *A&A*, 417, 839
- Le Fèvre, O., Vettolani, G., Garilli, B., et al. 2005, *A&A*, 439, 845
- Le Fèvre, O., Tasca, L. A. M., Cassata, P., et al. 2014, *A&A*, submitted  
[[arXiv:1403.3938](https://arxiv.org/abs/1403.3938)]
- Lilly, S. J., Le Fèvre, O., Renzini, A., et al. 2007, *ApJS*, 172, 70
- Lonsdale, C. J., Smith, H. E., Rowan-Robinson, M., et al. 2003, *PASP*, 115, 897
- Mauduit, J.-C., Lacy, M., Farrah, D., et al. 2012, *PASP*, 124, 1135
- Mas-Hesse, J. M., Kunth, D., Tenorio-Tagle, G., et al. 2003, *ApJ*, 598, 858
- Mallery, R. P., Mobasher, B., Capak, P., et al. 2012, *ApJ*, 760, 128
- Maraston, C., Pforr, J., Renzini, A., et al. 2010, *MNRAS*, 407, 830
- McCracken, H. J., Milvang-Jensen, B., Dunlop, J., et al. 2012, *A&A*, 544, A156
- Momose, R., Ouchi, M., Nakajima, K., et al. 2014, *MNRAS*, 442, 110
- Mostek, N., Coil, A. L., Moustakas, J., et al. 2012, *ApJ*, 746, 124
- Murayama, T., Taniguchi, Y., Scoville, N. Z., et al. 2007, *ApJS*, 172, 523
- Nilsson, K. K., Pietsch, W., Sala, G., et al. 2009, *A&A*, 498, 13
- Ono, Y., Ouchi, M., Mobasher, B., et al. 2012, *ApJ*, 744, 83
- Ouchi, M., Shimasaku, K., Akiyama, M., et al. 2008, *ApJS*, 176, 301
- Papovich, C., Finkelstein, S. L., Ferguson, H. C., et al. 2011, *MNRAS*, 412, 1123
- Partridge, R. B., & Peebles, J. E. 1967, *ApJ*, 147, 868
- Pentericci, L., Fontana, A., Vanzella, E., et al. 2011, *ApJ*, 743, 132
- Reddy, N. A., Steidel, C. C., & Erb, D. K. 2006, *ApJ*, 653, 100
- Reddy, N. A., Pettini, M., Steidel, C. C., et al. 2012, *ApJ*, 754, 25
- Sanders, D. B., Salvato, M., Aussel, H., et al. 2007, *ApJS*, 172, 86
- Schaerer, D. 2003, *A&A*, 397, 527
- Schaerer, D., de Barros, S., & Stark, D. P. 2011, *A&A*, 536, A72
- Scodreggio, M., Franzetti, P., Garilli, B., et al. 2005, *PASP*, 117, 1284
- Scoville, N., Aussel, H., Brusa, M., et al. 2007, *ApJS*, 172, 1
- Shapley, A., Dzhaliyov, N. S., Maltoni, M., et al. 2003, *ApJ*, 588, 65
- Schenker, M. A., Stark, D. P., Ellis, R. S., et al. 2012, *ApJ*, 744, 179
- Stark, D. P., Ellis, R. S., Chiu, K., et al. 2010, *MNRAS*, 408, 628
- Stark, D. P., Ellis, R. S., & Ouchi, M. 2011, *ApJ*, 728, 2
- Steidel, C. C., Adelberger, K. L., Giavalisco, M., et al. 1999, *ApJ*, 519, 1
- Steidel, C. C., Adelberger, K. L., Shapley, A. E., et al. 2000, *ApJ*, 532, 170
- Steidel, C. C., Bogosavljevic, M., Shapley, A. E., et al. 2011, *ApJ*, 736, 160
- Taniguchi, Y., Scoville, N., Murayama, T., et al. 2007, *ApJS*, 172, 9
- Tresse, L., Maddox, S., Loveday, J., & Singleton, C. 1999, *MNRAS*, 310, 262
- Utomo, D., Kriek, M., Labbé, I., et al. 2014, *ApJ*, 783, 30
- Vanzella, E., Pentericci, L., Fontana, A., et al. 2011, *ApJ*, 730, 35
- Verhamme, A., Schaerer, D., & Maselli, A. 2006, *A&A*, 460, 397
- Verhamme, A., Schaerer, D., Atek, H., & Tapken, C. 2008, *A&A*, 491, 89
- Verhamme, A., Dubois, Y., Blaizot, J., et al. 2012, *A&A*, 546, A111